



Optimal control of flow with discontinuities

Chris Homescu, I.M. Navon *

Department of Mathematics and C.S.I.T., Florida State University, Tallahassee, FL 32306, USA

Received 2 May 2002; received in revised form 21 February 2003; accepted 26 February 2003

Abstract

Optimal control of the 1-D Riemann problem of Euler equations is studied, with the initial values for pressure and density as control parameters. The least-squares type cost functional employs either distributed observations in time or observations calculated at the end of the assimilation window. Existence of solutions for the optimal control problem is proven. Smooth and nonsmooth optimization methods employ the numerical gradient (respectively, a subgradient) of the cost functional, obtained from the adjoint of the discrete forward model. The numerical flow obtained with the optimal initial conditions obtained from the nonsmooth minimization matches very well with the observations. The algorithm for smooth minimization converges for the shorter time horizon but fails to perform satisfactorily for the longer time horizon, except when the observations corresponding to shocks are detected and removed.

© 2003 Elsevier Science B.V. All rights reserved.

PACS: 65M32; 76N25

Keywords: Optimal control; Adjoint method; Nonsmooth optimization; LBFGS minimization; Euler equations; Discontinuity detection; Distributed observations

1. Introduction

Optimal control methods are presently employed for various applications in different fields: aerodynamics, meteorology, acoustics, financial mathematics and chemistry to mention but a few. Since the vast majority of applications consist of the minimization of a cost functional derived from continuous models, we have solved an optimization problem involving a cost functional for a discontinuous model. Our results show that, for the example considered, nonsmooth optimization methods provide very good results in combination with the adjoint method for subgradient computation.

Nondifferentiable optimization algorithms employing subgradients were introduced following the seminal work of Lemarechal [45] (e.g., [11,46,53,55,66] to cite but a few).

* Corresponding author. Tel.: +1-850-644-6560; fax: +1-850-644-0098.

E-mail addresses: homescu@cs.ucsb.edu (C. Homescu), navon@csit.fsu.edu (I.M. Navon).

URL: <http://www.csit.fsu.edu/~navon>.

Cost functionals involving a model with nonsmooth solution were employed in variational data assimilation in atmospheric sciences [79], for inverse design problems involving transonic diffusers: 1-D [60] or 2-D [20], in acoustics [34], for the research of a convex hull with bounded curvature of a given set of points [35], in mechanical structures (minimizing the maximal stress over an arch structure [33]), for chromatography [42], capital asset management [47], in the design of a duct flow with a shock [18,24,40], for airfoil design [28,39,43,58].

Although our model contains many types of discontinuities, we want to emphasize the fact that the nonsmoothness of a least-squares type cost functional (as considered in our research) appears only if the location of discontinuities of state and data coincide [29,73]. At a first glance, this would imply that smooth optimization methods may be suitable outside the region of nonsmoothness. But our numerical results show that this assertion is not valid in many cases, as opposed to nonsmooth optimization techniques, which were successful for all the considered cases.

In our opinion, this is closely related to the fact that the gradients computed using the numerical adjoint method are in a close neighborhood to the analytic gradient values, but they do not converge as the number of grid points increases. As consequence, they provided enough information for the subgradient methods, but not for the gradient-based methods.

Several other nongradient methods were considered for optimization problem derived from discontinuous models: e.g., stochastic optimization methods for the design of a minimum time changeover operation for a pressure vessel avoiding the formation of explosive mixtures [7] or for aerodynamic shape optimization [38], genetic algorithms [64] for wing optimization. For these methods, the drawback is the relatively large number of analyses required (i.e., large memory demands) as the number of variables increases.

In the case of gradient-based methods different remedies to alleviate the influence of the discontinuities were employed. For variables which are continuous across the shock one can avoid dealing with shocks by considering cost functions based on the above variables (e.g., the surface flux for inverse nozzle design as used by Matsuzawa and Hafez [57]). For most cases the shocks were smoothed using numerical dissipation. It was shown that sometimes smoothing is equivalent to modifying the cost function [57]. An alternative smoothing procedure has been introduced by Valorani and Dadone [71], namely a filtering process which was obtained by modifying a set of sensitivity equations by adding artificial dissipative terms. The optimization search was performed on the original nonsmooth objective function computed with an accurate (nonsmoothed) flow analysis but with smoothed flow sensitivities.

If the shocks are weak at design conditions (e.g., transonic flows) acceptable results can be obtained by addition of artificial dissipation. However, accurate treatment of the shock waves is essential in other cases (e.g., supersonic flows). The alternative approach to shock smearing is shock fitting which involves careful integration of the objective function through the shock wave [60]. Perturbation of a discontinuous function produces delta functions and formulations based on variations of smooth functions have to be modified [40]. Another approach was to introduce the shock location as an explicit control variable [18]. A coordinate straining method was also employed by Narducci et al. [60]. It consists of a coordinate transformation aimed at aligning the calculated shock with the target followed by addition of a penalty term proportional to the square of distance between the shocks.

Results for the optimal control of the Euler equations were obtained, among others, by Anderson and Venkatakrisnan [2] (in 2-D), Arian and Salas [4] (in 2-D), Dadone and Grossman [21,22] (2-D and 3-D) and Cliff et al. [16–18] (1-D, 2-D and 3-D).

Theoretical contributions (combined with practical applications in certain cases) for the adjoint method were provided by Giles and Pierce [25–28] (for Euler equations) and Ulbrich [72–75] (in the setting of optimal control for scalar conservation laws). A generalized adjoint for physical processes in atmospheric sciences with parameterized discontinuities was studied by Xu [78]. Numerical aspects of the adjoint model for discontinuous nonlinear atmospheric models were discussed by Zhang et al. [80].

Problems with discontinuities in an optimal control setting or in sensitivity-based control were studied by Mohammadi and Pironneau [59], Bardos and Pironneau [5,6], Gunzburger [31,32], Tolsma and Barton [70] and Zhang et al. [79]. Practical aspects of control of problems with shocks were presented by Iollo and Salas [41], Birkmeyer et al. [9], Stanewsky [69], Jameson [43], Bein et al. [8], or Wang et al. [77].

This paper presents theoretical and numerical results for an optimal control problem of the unsteady 1-D Riemann problem of Euler equations (shock-tube). The numerical solutions of the optimal control problem were obtained using both nonsmooth and smooth optimization algorithms. The present research extends our previous results in optimal control for a continuous flow [36] and sensitivity analysis for discontinuous flow [37].

This specific problem was chosen due to the fact that it has an analytical solution which is characterized by the presence of many types of discontinuities: shocks, contact discontinuities and wave rarefaction regions. This Riemann problem may be briefly described in the following way: a gas tube is divided by a membrane into two regions with different values for pressure and density fields and a zero velocity field. After the membrane is suddenly removed the gas moves freely.

Our optimal control problem consists of moving the regions of discontinuities to *desired* locations by matching the *desired* flow to the numerical flow. It has very interesting aerodynamic applications, since discontinuities in the flow variables during the flight have been shown to be related to the onset of flow separation, leading-edge vortex burst or the appearance–disappearance of more subtle flow structures [1,3]).

The control parameters consist of the initial values of pressure and density to the left and to the right of the membrane. We consider the initial velocity to the left and to the right of the membrane to be zero. The cost functional is the weighted difference between the *observations* and the numerical values for density, pressure and velocity fields. The observations obtained from the analytical solution of the Riemann problem are computed in two ways: either at the end of the assimilation window or distributed in time during the assimilation window.

Two numerical models were chosen, representative of possible approaches for solving a flow with discontinuities: a high-resolution model (HRM) and a model with artificial viscosity (AVM).

We employ a nonsmooth optimization algorithm described in [53,54,76], which is a hybrid algorithm that combines the characteristics of the variable metric method and the bundle method. We also apply a smooth optimization algorithm (L-BFGS) described in [51,62]. Both methods require the computation of a subgradient (respectively, the gradient) of the cost functional. This subgradient (respectively, gradient) is obtained from the adjoint model derived from the original numerical model.

We consider two time horizons representative for the time evolution of the flow. The selection of the length of the time horizons was based on two requirements. We wanted to ensure that all desired characteristics of the discontinuities are still present in the flow at the end of each time window. Moreover, if one would slightly increase the larger time window then some of the discontinuity characteristics will disappear from the spatial domain considered.

We obtained excellent results using nonsmooth optimization for both models and for both time horizons. The numerical flow corresponding to the *optimized* initial conditions matches closely the observations and one can see from the figures presented that the location of the discontinuities was changed to the *desired* location. The figures describing the evolution of entropy at various stages of the minimization process show that the numerical solution satisfies the entropy condition, which is a required characteristic of the physical solution of the shock-tube problem.

The L-BFGS algorithm did not converge in many cases. Even for the cases where convergence was obtained one may notice a large difference between the L-BFGS optimization results and the *desired* values of the control parameters. One of the main reasons for this behavior is the fact that the numerical values of the gradient do not match very well the analytical values, even as the number of grid points increases.

For the model with artificial viscosity a discontinuity detection method was used to eliminate the points where the shock is located from the computation of the cost functional and its gradient (or subgradient).

As a result of this technique the optimized results were obtained at the same level of accuracy but in fewer minimization iterations.

The paper is organized as follows. Section 2 introduces the governing equations (unsteady Euler 1-D) for the flow. Section 3 describes the discretization of the 1-D Riemann problem in space and time using both the high-resolution model and the artificial viscosity model. In Section 4 we present results related to existence of solutions for optimal control problem considered. Section 5 discusses methods of nonsmooth and smooth unconstrained optimization employed for this research. Methods of detection of discontinuities in data are presented in Section 6. Numerical results obtained for the optimal control problem of 1-D Euler equations are displayed in the tables and figures of Section 7. Section 7 also discusses the evolution of the cost functional for both methods of minimization, both models and both time horizons considered. Finally Section 8 presents the summary and conclusions.

2. Governing equations

The one-dimensional unsteady equations of gas dynamics (Euler equations) can be written in conservation law form as

$$\mathbf{U}_t + \mathbf{F}(\mathbf{U})_x = 0, \quad \mathbf{U} = \begin{bmatrix} \rho \\ m \\ e \end{bmatrix}, \quad \mathbf{F}(\mathbf{U}) = \begin{bmatrix} m \\ \frac{m^2}{\rho} + P \\ \left(\frac{m}{\rho}\right)(e + P) \end{bmatrix}, \quad (1)$$

where ρ is the density, u is the velocity, $m = \rho u$ is the momentum, P is the pressure and e is the internal energy per unit volume. The variables are related by $e = \rho \varepsilon + \frac{1}{2} \rho u^2$, where $\varepsilon = P/((\gamma - 1)\rho)$ is the internal energy per internal mass with γ the ratio of specific heats (which is taken to be 1.4).

The “shock-tube problem” can be described as follows: a tube, filled with gas, is initially divided by a membrane into two sections. The gas has a higher density and pressure in one half of the tube than in the other half, with zero velocity everywhere. The initial conditions for density, velocity and pressure are similar to the values for the Sod shock-tube problem [68],

$$\rho_{\text{left}} = 1.0 > \rho_{\text{right}} = 0.125, \quad u_{\text{left}} = u_{\text{right}} = 0.0, \quad p_{\text{left}} = 1.0 > p_{\text{right}} = 0.1,$$

where the subscripts left and right correspond to the initial position with respect to the membrane. At time $t = 0$ the membrane is suddenly removed and the gas is allowed to flow. We expect a net motion in the direction of lower pressure. Assuming uniform flow across the tube, there is variation in only one direction and 1-D Euler equations apply. The flow variables: pressure, density and velocity are computed as a function of time and space.

We consider the spatial domain to be the interval $[0, 1]$. The boundary conditions are specified as follows: the boundary values for U (at $x = 0$ and $x = 1$) do not change throughout the process.

The solution of this Riemann problem for Euler equations [50] consists of five distinct regions as shown in Figs. 1 and 3: low pressure and density region (region 1), area between shock and contact discontinuity (region 2), area between contact discontinuity and rarefaction wave (region 3), rarefaction wave region (region R) and high pressure and density region (region 4).

3. Numerical models

The main difficulties encountered when solving numerically the shock-tube problem of gas dynamics (and, in general, for any problem which has a nonsmooth solution) appear in the regions of discontinuities. The numerical solution may be smoothed in those regions (e.g., due to introduction of a dissipation term)

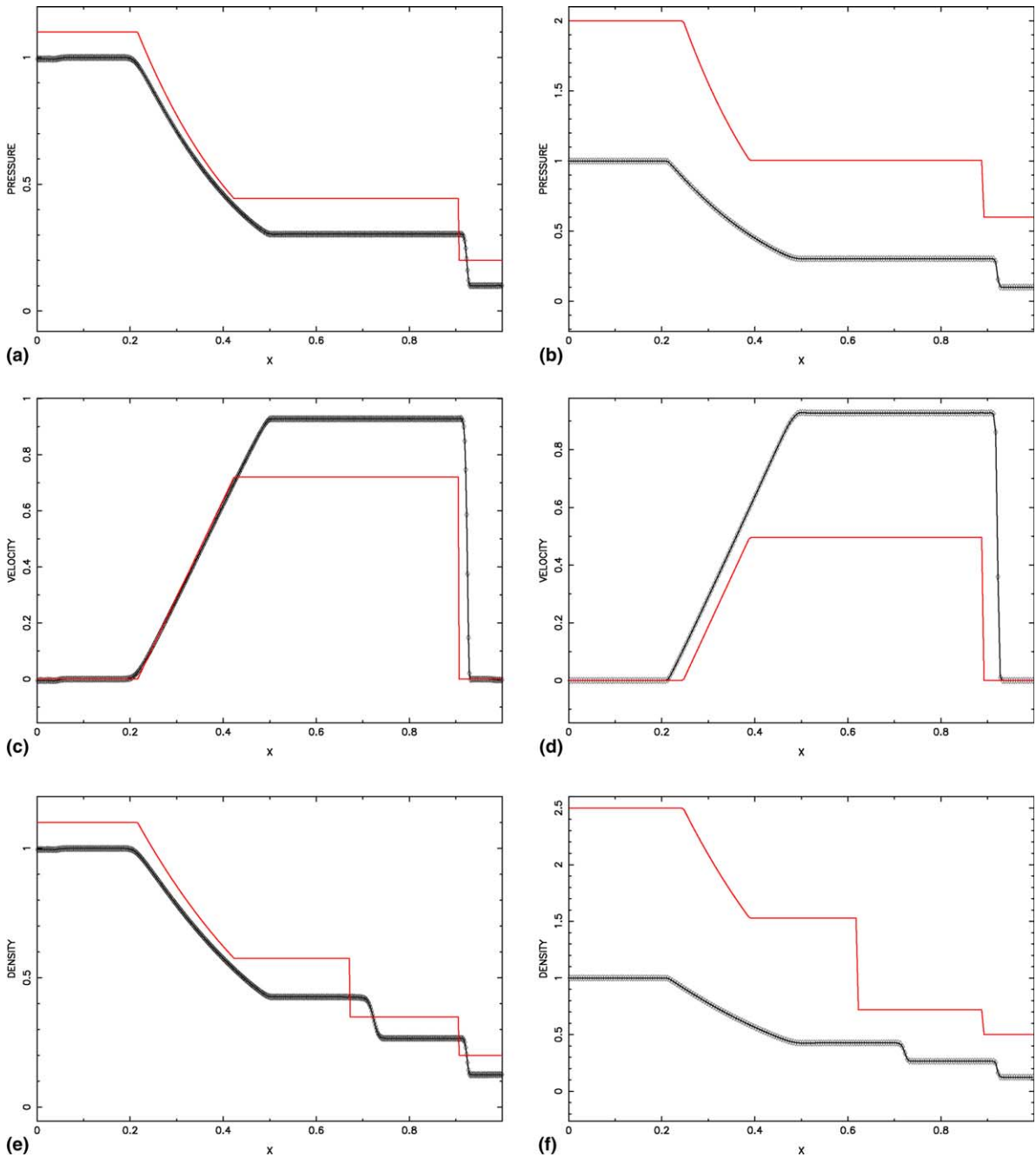


Fig. 1. Pressure, velocity and density: initial guess (\diamond) and exact observation (thin line) at time = 0.24 for the artificial viscosity model and first set of observations (a), (c), (e) and for the high-resolution model and the second set of observations (b), (d) and (f).

or it can sharpen discontinuities (using high-resolution methods). For this reason we chose one numerical model from each of the above mentioned categories: namely a model with artificial viscosity (AVM) and a high-resolution model (HRM) with a Riemann solver.

As a footnote we mention that for very accurate numerical solutions adaptive mesh refinement AMR may be used in conjunction with Riemann solvers (e.g., [49] for Euler equations). Our experience with an AMR model in the framework of sensitivity analysis for discontinuous flows was presented in [37].

Our research aims to perform optimal control of flow with discontinuities using either smooth or nonsmooth optimization techniques for minimizing the cost functional. The minimization requires availability of either the gradient or the subgradients of the cost functional obtained, using the adjoint model derived from the forward model (either AVM or HRM models).

The first model (by Cowan [19]) uses finite elements which are piecewise constant in time and piecewise linear in space. The elements are discontinuous in time but continuous in space. By using discontinuous discretization in time we were able to march sequentially in time and solve for only a fraction of the total solution at one time. To improve the stability of the method a least-squares operator was added to the basic Galerkin formulation. In order to obtain nonoscillatory approximations to discontinuities, discontinuity-capturing operators have been developed within the framework of this Galerkin/least-squares method. For more details about this modified discontinuous Galerkin method the reader is referred to [67]. An artificial viscosity term was included to stabilize the numerical solution with the effect of spreading flow discontinuities over several computational cells. The method employs a high-order scheme for the smooth regions of the flow combined with a low-order solution which is employed near the discontinuities. The above combination is described in [52] as MC-ML method (with the high-order scheme using a consistent mass matrix while the low-order scheme employs a lumped mass matrix).

The second model employs Roe's approximate Riemann solver combined with an entropy fix [48] and it is a component of the package CLAWPACK [49].

4. Theoretical framework of the optimal control problem

We solve the following optimal control problem:

$$\text{Minimize the cost functional } \mathbf{J}(q, z) \text{ subject to } z \in \mathcal{U}_{\text{ad}} \quad (\text{OPT})$$

where z is the control, \mathcal{U}_{ad} is the space of admissible controls and $q = q(z)$ is the entropy solution of the Cauchy problem for a system of conservation laws (Euler 1-D equations described in the previous section):

$$\frac{\partial q}{\partial t} + \frac{\partial F(q)}{\partial x} = 0, \quad (2)$$

$$q(x, 0) = z(x), \quad (3)$$

with $0 \leq t \leq T_w$ (the length of the assimilation window).

Since the solution of the system (2) may develop discontinuities after a finite time, weak solutions should be considered. Additional entropy conditions must be imposed to select the “physically” relevant weak solution.

An entropy function is defined and an additional conservation law holds for it for smooth solutions. This conservation law becomes an inequality for discontinuous solutions [30,48]). It is known that for the Euler equations of gas dynamics (employed for this research) there exists a physical quantity (the entropy), known to be constant along particle paths in smooth flow and to jump to higher value as the gas crosses a shock. The correct weak solution is picked out using a property of the entropy, namely that it can never jump to a lower value (a numerical version of this approach was employed for the high resolution model described in the previous section). The numerical evolution of the physical entropy is described in Section 7.

For the system of gas dynamics equations, which is a strictly hyperbolic symmetrizable nonlinear system of conservation laws, entropy functions can be found (e.g., [30,48]).

We will follow here the approach of Ulbrich [74] to derive existence results for optimal controls. His work, related to scalar laws of conservation with source terms, can be extended to our case (the 1-D system of Euler equations without source terms).

For our problem the control vector $z(x)$ is

$$z(x) = \begin{bmatrix} \rho(x, 0) \\ m(x, 0) \\ e(x, 0) \end{bmatrix} = \begin{bmatrix} \rho(x, 0) \\ \rho(x, 0)u(x, 0) \\ \frac{P(x,0)}{(\gamma-1)} + \frac{1}{2}\rho(x, 0)(u(x, 0))^2 \end{bmatrix},$$

with ρ the density, u the velocity, $m = \rho u$, P the pressure, γ the ratio of specific heats and e the internal energy per unit volume.

We consider that the controls (initial data) are in $(\mathbf{L}^1[0, 1])^3$ with small total variation. In this case, Bressan and his collaborators showed that the weak solutions of the conservation laws depend continuously on the initial values, with a Lipschitz constant in \mathbf{L}^1 which is uniform w.r.t time. Moreover, they obtained \mathbf{L}^1 -stability for initial data [12–14].

If the control problem (OPT) is particularized to the optimal control problem for 1-D Euler equations for gas dynamics (described in Section 2), the existence of the optimal controls is obtained as a consequence of three properties described below. In our research the cost functional \mathbf{J} for the optimal control problem (OPT) assumes two possible forms:

- If the observations q^{obs} are obtained only for the final time T_w

$$\mathbf{J}(q) = \int_0^1 (q(x, T_w) - q^{\text{obs}}(x, T_w))^2 dx. \tag{4}$$

- If the observations q^{obs} are distributed at assimilation times $0 \leq t \leq T_w$

$$\mathbf{J}(q) = \int_{t=0}^{t=T_w} \int_{x=0}^{x=1} (q(x, t) - q^{\text{obs}}(x, t))^2 dx dt. \tag{5}$$

Then, the existence of the optimal controls for the optimal control problem for 1-D Euler equations for gas dynamics is obtained as a consequence of several properties described below.

(P1) The function \mathbf{F} (in 1-D Euler equations for gas dynamics) is locally Lipschitz.

(P2) Denoting $\text{BV}(0, 1)$ the space of functions of bounded variations on the interval $(0, 1)$, the admissible set \mathcal{U}_{ad} is bounded in $\text{BV}(0, 1)$ and compact in $(\mathbf{L}^1(0, 1))^3$.

(P3) The cost functional \mathbf{J} is (at least) sequentially lower semicontinuous.

Using the properties (P1)–(P3) one can prove that the optimal control problem (OPT) has a solution $\hat{z} \in \mathcal{U}_{\text{ad}}$ in a similar way to the proof of existence of optimal controls obtained by Ulbrich [74].

First we prove that if \mathbf{J} satisfies (P3) then

$$z \in (\mathcal{U}_{\text{ad}} \subset (\mathbf{L}^1(0, 1))^3) \hookrightarrow \mathbf{J}(q(z), z) \tag{6}$$

is sequentially lower semicontinuous.

Indeed, let the sequence $(z^k) \subset \mathcal{U}_{\text{ad}}$ converge in $(\mathbf{L}^1[0, 1])^3$ to z_0 . We have that $z_0 \in \mathcal{U}_{\text{ad}}$ using property (P2). Bressan et al. [14] proved that weak solution obtained as limit of front tracking approximations depends Lipschitz continuously on the initial data, which implies that $q(z^k) \rightarrow q(z_0)$ in $\mathbf{C}([0, T_w]; \mathbf{L}^1)$. It follows from property (P3) that

$$\liminf_{k \rightarrow \infty} \mathbf{J}(q(z^k), z^k) \geq \mathbf{J}(q(z_0), z_0),$$

which establishes the lower semicontinuity of the operator defined in (6).

Finally let (z^j) be a minimizing sequence for the optimal control problem (OPT). Using compactness of \mathcal{U}_{ad} there exists a subsequence which converges to $\hat{z} \in \mathcal{U}_{ad}$. We have proved that the operator (6) is sequentially lower semicontinuous, which implies that \hat{z} is a solution for the optimal control problem (OPT). This concludes the proof of existence of solutions for (OPT).

5. Minimization algorithms

In order to minimize the above described cost functional we employed both nonsmooth and smooth optimization algorithms. A brief description of specific algorithms from each class implemented in this research is provided in the following two subsections.

5.1. Nonsmooth optimization: hybrid method

Since the gradient of a Lipschitz-continuous function f exists only almost anywhere we have to replace the gradient by the generalized gradient

$$\partial f(x) = \text{conv}\{g\} \text{ there exists a sequence } (x_i)_{i \in \mathbf{N}} \text{ such that } \lim_{i \rightarrow \infty} x_i = x, f \text{ differentiable at } x_i, \\ i \in \mathbf{N} \text{ and } \lim_{i \rightarrow \infty} \nabla f(x_i) = g\},$$

where “conv” is the notation for the convex hull.

We assume that we can compute the value of the function and an arbitrary subgradient $g \in \partial f(x)$ (i.e., one element of the generalized gradient) at any point in the domain.

The most efficient globally convergent algorithms for nonconvex nonsmooth optimization are based on versions of the bundle methods (e.g., [11,46,55,66]). We employed a hybrid method (described in [54,76]) which combines the characteristics of the variable metric method and the bundle method.

The algorithm generates a sequence of basic points $(x_k)_{k \in \mathbf{N}}$ and a sequence of trial points $(y_k)_{k \in \mathbf{N}}$ satisfying

$$x_{k+1} = x_k + t_L^k d_k, \quad y_{k+1} = x_k + t_R^k d_k, \quad y_1 = x_1,$$

where $t_R^k \in (0, t_{\max}]$ and $t_L^k \in [0, t_R^k]$ are appropriately chosen stepsizes, $d_k = -H_k \tilde{g}_k$ is a direction vector, \tilde{g}_k is an aggregate subgradient and the matrix H_k accumulates information about the previous subgradients and represents an approximation of the inverse Hessian matrix if the function f is smooth.

If the descent condition

$$f(y_{k+1}) \leq f(x_k) - c_L t_R^k w_k$$

is satisfied with suitable t_R^k , where $c_L \in (0, 0.5)$ is fixed and $-w_k < 0$ represents the desirable amount of descent, then $x_{k+1} = y_{k+1}$ (descent step). Otherwise a null step is taken which keeps the basic points unchanged but accumulates information about the minimized function.

The aggregation is defined in the following way: denoting by m the lowest index j satisfying $x_j = x_k$ (index of the iteration after last descent step) and having the basic subgradient $g_m \in \partial f(x_k)$, the trial subgradient $g_{k+1} \in \partial f(y_{k+1})$ and the current aggregate subgradient \tilde{g}_k , we define \tilde{g}_{k+1} as a convex combination of these subgradients:

$$\tilde{g}_{k+1} = \lambda_{k,1} g_m + \lambda_{k,2} g_{k+1} + \lambda_{k,3} \tilde{g}_k,$$

where λ_k are determined by minimizing a simple quadratic function depending on these three subgradients and two subgradient locality measures (this approach replaces solving a rather complicated quadratic programming problem which appears in the standard bundle method [46]).

The matrices H_k are generated using a symmetric quasi-Newton rank-one update after the null steps (to preserve the property of being bounded and other characteristics required for the global convergence) or the standard BFGS update after the descent steps (for both types of updates see [23]).

5.2. The L-BFGS unconstrained optimization algorithm

We also implemented the L-BFGS method ([51,62,63]) which performs the unconstrained minimization of a smooth nonlinear function for which the gradient is available. L-BFGS is a limited memory method based on the well-known BFGS (Broyden–Fletcher–Goldfarb–Shanno) algorithm.

The main idea of this method is to use curvature information only from the most recent iterations to construct the Hessian approximation. Instead of storing fully dense $n \times n$ approximations it saves just a few vectors of length n that represent the approximations implicitly.

Each step of the original BFGS method has the form

$$x_{k+1} = x_k - \alpha_k H_k \nabla J_k, \quad k = 0, 1, 2, \dots,$$

where α_k is the step length and J_k is the cost functional at step k of the minimization iteration. H_k is updated at each iteration by means of the formula

$$H_{k+1} = V_k^T H_k V_k + \beta_k s_k s_k^T, \quad (7)$$

$$\beta_k = \frac{1}{y_k^T s_k}, \quad V_k = I - \beta_k y_k s_k^T, \quad (8)$$

$$s_k = x_{k+1} - x_k, \quad y_k = \nabla J_{k+1} - \nabla J_k. \quad (9)$$

The matrix H_{k+1} is obtained by updating H_k using the pair (s_k, y_k) . For L-BFGS a modified version of H_k is stored implicitly by using a certain number (say m) of the vector pairs (s_l, y_l) that are used in the formulae (7)–(9).

The product $H_k \nabla J_k$ can be obtained by performing a sequence of inner products and vector summations involving ∇J_k and the pairs (s_l, y_l) . After the new iterate is computed, the oldest vector pair in the set of pairs (s_l, y_l) is deleted and replaced by the new pair (s_k, y_k) obtained from the current step (9). In this way the set of vector pairs includes curvature information from the m most recent iterations (usually $3 \leq m \leq 10$).

For numerical experience using the L-BFGS method the reader is referred to [81].

We would like to conclude this section discussing our preference for L-BFGS over other smooth minimization algorithms. One may argue that for our case the number of control parameters may not justify the selection of a limited memory method. We consider that our approach (using the adjoint method for the gradient computation) may be easily and successfully implemented for optimal control problems in higher dimensions with a much greater number of control variables. In that case improvements in the efficiency of the numerical optimization will be determined not only by choosing the adjoint method over other methods for the gradient calculation but also by selecting a limited memory minimization algorithm.

6. Detection of discontinuities in data

In the setting of smooth minimization one may consider that, by eliminating the observations corresponding to discontinuities from the computation of the cost functional, one may obtain a function which is smoother (i.e., more suitable for smooth optimization). Several approaches can be found in literature for the detection of discontinuities.

The discontinuity locking system (DLS) is employed for differential-algebraic equations (DAE) by Birta and Oren [10], Park and Barton [65] and Mao and Petzold [56], to cite but a few. The idea for this approach (DLS) is to lock the function evaluator for the initial-value problem solver so that the equations evaluated are fixed while an integration step is being taken, thus presenting a smooth vector field to the solver.

The approach we employ here is a modified application of a discrete regularization method proposed by Lee and Pavlidis [44]. Let $(x_i, y_i)_{i=0, \dots, n}$ be the set of data points with $x_i < x_{i+1}$. We want to find the $n + 1$ quantities z_i that minimize a combination of the discrete curvature and the discrete difference between observation and desired data,

$$\sum_{i=0}^n \alpha_i \left(\frac{z_{i+1} - z_i}{x_{i+1} - x_i} - \frac{z_i - z_{i-1}}{x_i - x_{i-1}} \right)^2 + \beta \sum_{i=0}^n (z_i - y_i)^2, \quad (10)$$

with $\alpha_0 = \alpha_n = 0$ and $\alpha_i = 1$ for $i = 1, \dots, n - 1$.

Differentiating (10) with respect to z_k and setting the derivatives to zero yields a system of $n + 1$ equations with $n + 1$ variables. The parameter β is chosen such that it satisfies: $\beta \gg 1/(\min_k (x_{k+1} - x_k)^2)$ which implies diagonal dominance for the derived system of equations.

As a result of solving this system we obtain a set of data points $(x_i, z_i)_{i=0, \dots, n}$ which are used for discontinuity detection for both the function and its derivative.

Let us consider the following quantities:

$\text{error}(i) = z_i - y_i$ difference between observation and desired data

$\text{curv}(i) = \frac{z_{i+1} - z_i}{x_{i+1} - x_i} - \frac{z_i - z_{i-1}}{x_i - x_{i-1}}$ approximation of the curvature

Discontinuities in the derivative of the function are characterized by successive zero crossings of $\text{curv}(i)$ while function discontinuities are characterized by successive zero crossings of $\text{curv}(i)$ and $\text{error}(i)$.

Consequently, in the interval $[x_i, x_{i+1}]$ we have function discontinuities the points if $\text{curv}(i) \times \text{curv}(i + 1) < -\epsilon$ and $\text{error}(i) \times \text{error}(i + 1) < -\epsilon$, where ϵ depends on the accuracy of the model.

7. Numerical results

Our goal was to control the location of the discontinuities by matching the numerical flow to observations corresponding to a flow which contains the *desired* location of discontinuities.

For many problems (including ours) the problem of finding a “matching” flow at a given time is equivalent to the problem of finding the corresponding vector of initial conditions (the initial conditions serve as the control variables in the optimal control setting).

For practical applications of this approach (namely controlling the location of the discontinuities) it is more important to consider the impact on flow parameters due to the change of shock location rather than the explicit description of the *new* discontinuity location. For this reason we concentrated our research efforts on matching the flow to a *desired* flow rather than introducing the explicit shock location as a variable in the optimal control setup (as performed by Cliff et al. [18] for duct flow with quasi 1-D Euler equations).

We used the discrete forward model to obtain the tangent linear model and then the adjoint model which provides the gradient or a subgradient of the cost functional to the smooth (nonsmooth) minimizer. If the

location of the discontinuities were to be introduced as an explicit variable, then the original model should be modified to accommodate the new requirements, a change requiring complex adjustments. For this reason we consider our approach more suitable for practical optimization problems involving discontinuities.

We considered as forward models an artificial viscosity model AVM and a high-resolution model HRM. For each of the two numerical models we employed unconstrained optimization methods (L-BFGS algorithm for smooth optimization and PVAR algorithm for nonsmooth optimization) described in Section 5.

The control variables were chosen to be the initial parameters to the left and to the right of the membrane: pressure p_L, p_R and density ρ_L, ρ_R . The desired observations were obtained as exact solutions of the shock-tube problem at times $t = 0.15$ or 0.24 starting with prescribed initial conditions. We considered two set of parameters: (ONE) and (TWO):

$$\text{ONE} = [\rho_L = 1.1, p_L = 1.1, \rho_R = 0.2, p_R = 0.2],$$

$$\text{TWO} = [\rho_L = 2.5, p_L = 2.0, \rho_R = 0.5, p_R = 0.6].$$

The initial guess for both minimization methods (INIT) is characteristic for the Sod shock-tube problem ([68]),

$$\text{INIT} = [\rho_L = 1.0, p_L = 1.0, \rho_R = 0.1, p_R = 0.1].$$

The initial values for velocities to the left and to the right of the membrane were taken to be zero.

The numerical results for both models (AVM and HRM) using each of the optimization methods (L-BFGS and PVAR) are presented in Fig. 2 (the evolution of the cost functional vs. the number of minimization iterations) as well as Fig. 3 (the numerical flow obtained using the results of optimization compared with the observations). The values of the optimized control parameters are presented in Table 3 (HRM) and Table 4 (AVM). We considered two different time horizons for the optimal control problem: $T_w = 0.15$ or 0.24 (in nondimensional units). They were chosen for two main reasons. First, at the end of the time window the flow exhibits all five regions of discontinuities previously discussed in Section 2. Second, if one increases the time horizon from $T_w = 0.24$ to a slightly larger value $time = 0.3$ one can see from Fig. 4 that several characteristics of the discontinuities have already disappeared from the spatial domain considered.

As discussed in Section 4 we consider two expressions for the cost functional, with observations located either at the end of the assimilation window or with distributed observations in time.

When the observations were located at the end of the time window ($t = T_w$) the following discrete form of the cost functional was considered:

$$J(\mathbf{U}(\cdot, 0), \mathbf{P}(\cdot, 0), \rho(\cdot, 0)) = \sum_{i=1}^{N_p} \left(W_U(i) (\mathbf{U}^{\text{num}}(i) - \mathbf{U}^{\text{obs}}(i))^2 + W_P(i) (\mathbf{P}^{\text{num}}(i) - \mathbf{P}^{\text{obs}}(i))^2 + W_\rho(i) (\rho^{\text{num}}(i) - \rho^{\text{obs}}(i))^2 \right),$$

where

$$\mathbf{U}(x, 0) = \begin{cases} 0.0, & x < 0.5 \\ 0.0, & x > 0.5 \end{cases}, \quad \mathbf{P}(x, 0) = \begin{cases} p_L, & x < 0.5 \\ p_R, & x > 0.5 \end{cases}, \quad \rho(x, 0) = \begin{cases} \rho_L, & x < 0.5 \\ \rho_R, & x > 0.5 \end{cases},$$

with $(\rho_L, p_L, \rho_R, p_R)$ the control variables described above. N_p is the number of points for space discretization, W_U, W_P, W_ρ are weights matrices attached to points (the identity matrix in our implementation).

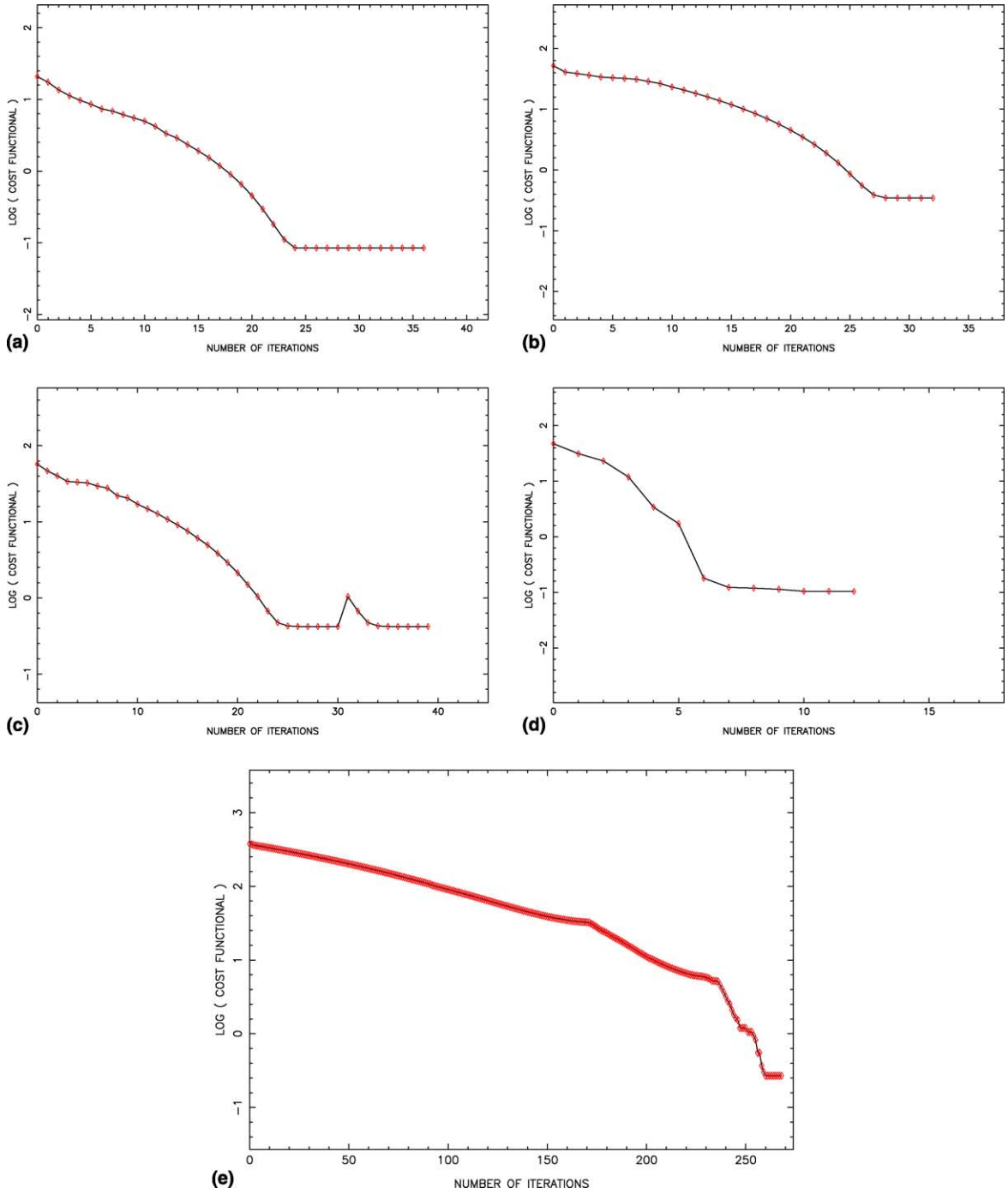


Fig. 2. Evolution of the logarithm of cost functional vs. number of iterations at time = 0.24 for HRM: PVAR + first set of observations without (a) or with (b) distributed observations; PVAR + second set of observations (c) and, respectively, for AVM (PVAR + first set of observations (d); L-BFGS with discontinuity detection and term removal and first set of observations (e).

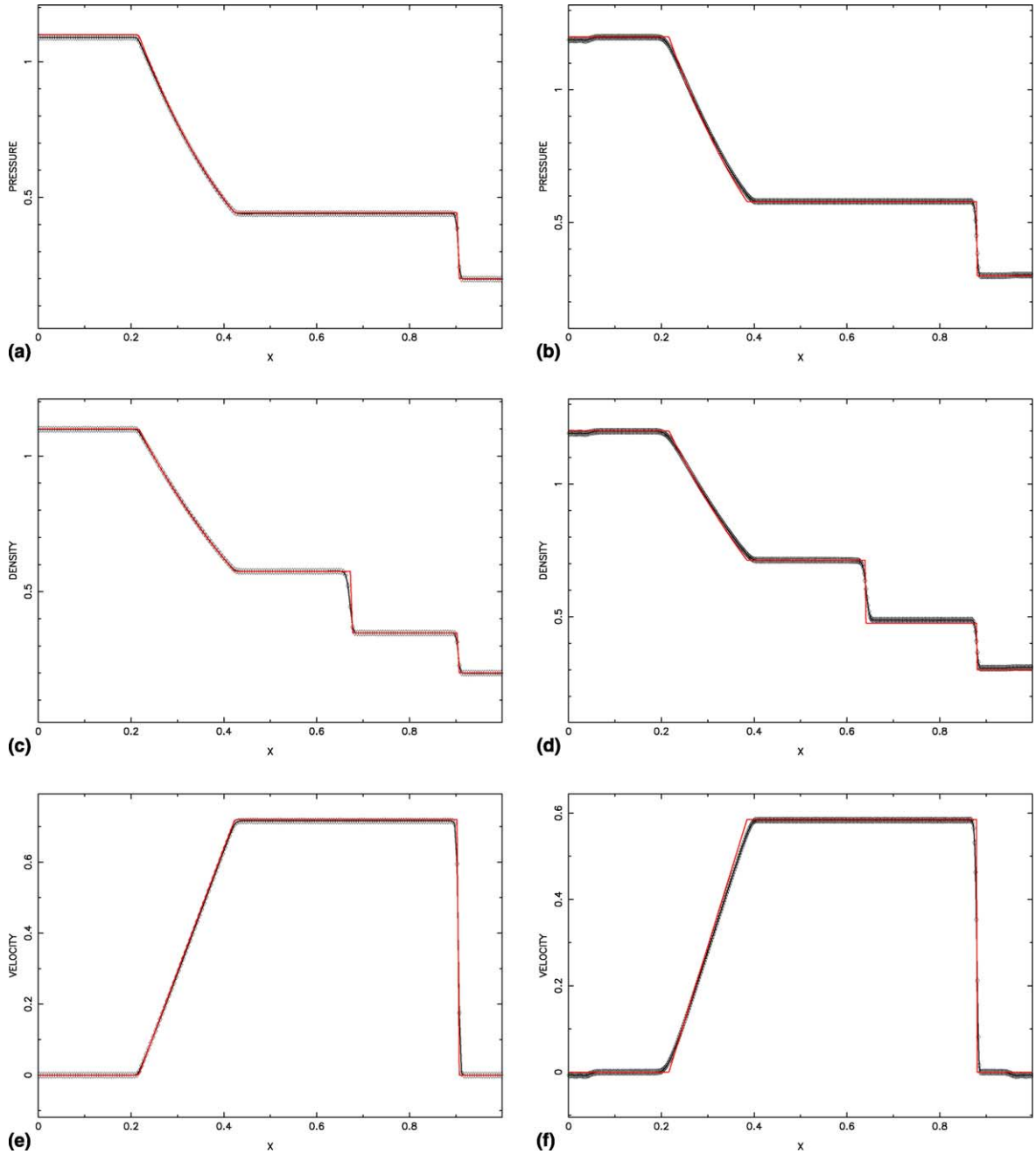


Fig. 3. Pressure, density and velocity: observations (thin line) and numerical solution (\diamond) at time $t=0.24$ for the first set of observations HRM (PVAR (a), (c) and (e)) and, respectively, for AVM (L-BFGS with discontinuity detection and term removal (b), (d) and (f)).

\mathbf{U}^{num} , \mathbf{P}^{num} , ρ^{num} are the fields of velocity, pressure and density at time t_{final} while \mathbf{U}^{obs} , \mathbf{P}^{obs} , ρ^{obs} are the observations for velocity, pressure and density.

Table 1

Gradient of the cost functional with respect to the control variables for the high-resolution model

	100 points	200 points	400 points	500 points	Exact value
ρ_L	0.910031588	0.900192636	0.893206369	0.894630746	0.922092236
ρ_R	0.792576124	0.765652869	0.742964725	0.741700828	0.711993332
p_L	0.426147283	0.259507114	0.138748378	0.162920439	0.511979175
p_R	0.398853592	0.530988984	0.627920012	0.615861264	0.568648995

Table 2

Gradient of the cost functional with respect to the control variables for the artificial viscosity model

	200 points	400 points	500 points	1000 points	Exact value
ρ_L	0.906984749	0.900370054	0.899532462	0.898418391	0.922092236
ρ_R	0.593117245	0.589481465	0.588288589	0.583323087	0.711993332
p_L	0.205244621	0.198562144	0.201226646	0.236071976	0.511979175
p_R	0.737312984	0.745349578	0.745462328	0.732442672	0.568648995

Table 3

Optimization results for the high-resolution model

Parameter	ρ_L	p_L	ρ_R	p_R
<i>First set of observations and time = 0.15</i>				
Desired	1.1	1.1	0.2	0.2
L-BFGS	1.10143	1.10251	0.19934	0.19865
PVAR	1.10059	1.10187	0.19942	0.19884
<i>First set of observations and time = 0.24</i>				
Desired	1.1	1.1	0.2	0.2
L-BFGS	Failed	Failed	Failed	Failed
PVAR	1.09815	1.08966	0.19993	0.19894
PVAR [d.o.]	1.10088	1.10915	0.20122	0.19886
<i>Second set of observations and time = 0.24</i>				
Desired	2.5	2.0	0.5	0.6
PVAR	2.49591	1.97919	0.49941	0.60096

For distributed observations the discrete form of the cost functional is

$$J(\mathbf{U}(\cdot, 0), \mathbf{P}(\cdot, 0), \rho(\cdot, 0)) = \sum_{j=1}^{N_{\text{obs}}} \sum_{i=1}^{N_p} \left(W_U(i) \left(\mathbf{U}_{(j)}^{\text{num}}(i) - \mathbf{U}_{(j)}^{\text{obs}}(i) \right)^2 + W_P(i) \left(\mathbf{P}_{(j)}^{\text{num}}(i) - \mathbf{P}_{(j)}^{\text{obs}}(i) \right)^2 + W_\rho(i) \left(\rho_{(j)}^{\text{num}}(i) - \rho_{(j)}^{\text{obs}}(i) \right)^2 \right).$$

In addition to the notations for the previous cost functional we denote by N_{obs} the number of instances when the observations are determined during the assimilation window, $\mathbf{U}_{(j)}^{\text{num}}$, $\mathbf{P}_{(j)}^{\text{num}}$, $\rho_{(j)}^{\text{num}}$ are the fields of velocity, pressure and density at time $t_{(j)}$, while $\mathbf{U}_{(j)}^{\text{obs}}$, $\mathbf{P}_{(j)}^{\text{obs}}$, $\rho_{(j)}^{\text{obs}}$ are the observations for velocity, pressure and density at the same observation times $t_{(j)}$ with $1 \leq j \leq N_{\text{obs}}$.

Table 4
Optimization results for the artificial viscosity model

Parameter	ρ_L	p_L	ρ_R	p_R
<i>First set of observations and time = 0.15</i>				
Desired	1.1	1.1	0.2	0.2
L-BFGS	1.09712	1.09947	0.20432	0.19756
L-BFGS [t.r.]	1.10031	1.10459	0.20514	0.19786
PVAR	1.09685	1.09933	0.20439	0.19782
<i>First set of observations and time = 0.24</i>				
Desired	1.1	1.1	0.2	0.2
L-BFGS	1.02638	1.00347	0.18012	0.19296
L-BFGS [t.r.]	1.09742	1.10173	0.20004	0.20154
PVAR	1.09737	1.09966	0.20357	0.19874
PVAR [input]	1.09741	1.09961	0.20344	0.19867
<i>Second set of observations and time = 0.24</i>				
Desired	2.5	2.0	0.5	0.6
PVAR	2.488763	1.964391	0.4867374	0.6241672

7.1. Numerical results for the high-resolution model HRM

For the HRM model the optimized values of the control parameters are in excellent agreement with the parameters' *desired* values for both assimilation windows when the nonsmooth optimization package PVAR was employed. Fig. 2 shows a decrease of more than two orders of magnitude for the cost functional. The *optimized* values of the control parameters [ρ_L , p_L , ρ_R , p_R] obtained as a result of nonsmooth minimization (the row PVAR in Table 3) display a very good agreement with the *desired* parameters. This remark is also supported by Fig. 3, which presents the comparison between the numerical *optimized* solution and the observations.

For the model HRM we also employed a cost functional with time-distributed observations for the larger time window $T_W = 0.24$. The optimized values of the control parameters obtained as a result of the nonsmooth minimization are shown as entries in the column PVAR [d.o.] (distributed observations) in Table 3. Since we have already obtained *optimized* results almost identical to the *desired* values of the parameters using only final time observations, the additional information provided by time-distributed observations was extraneous. Although it does not have any major impact for our problem, we wanted to prove that our methodology is successful also for the time-distributed approach, which is common for large-scale optimization problems in atmospheric sciences (e.g., [61]).

To verify the robustness of our approach we considered the second set of parameters (TWO). The results obtained using nonsmooth optimization PVAR (also shown in Table 3) are in very good agreement with the *desired* values of the parameters. Fig. 4 shows that the flow obtained with the *optimized* control parameters as initial conditions matches closely the observations. It also shows that the new location of discontinuities matches the *desired* location.

The evolution of the entropy during various stages of the minimization process (computed at the end of the assimilation window) is displayed in Fig. 5. It is known that the correct weak solution should satisfy the entropy condition, which states that the entropy of fluid particles does not decrease. Over the contact discontinuity the entropy decreases, but since fluid particles do not cross the contact discontinuity, the entropy of the particles does not decrease. This shows that the numerical solution has indeed the characteristics of a physical solution.

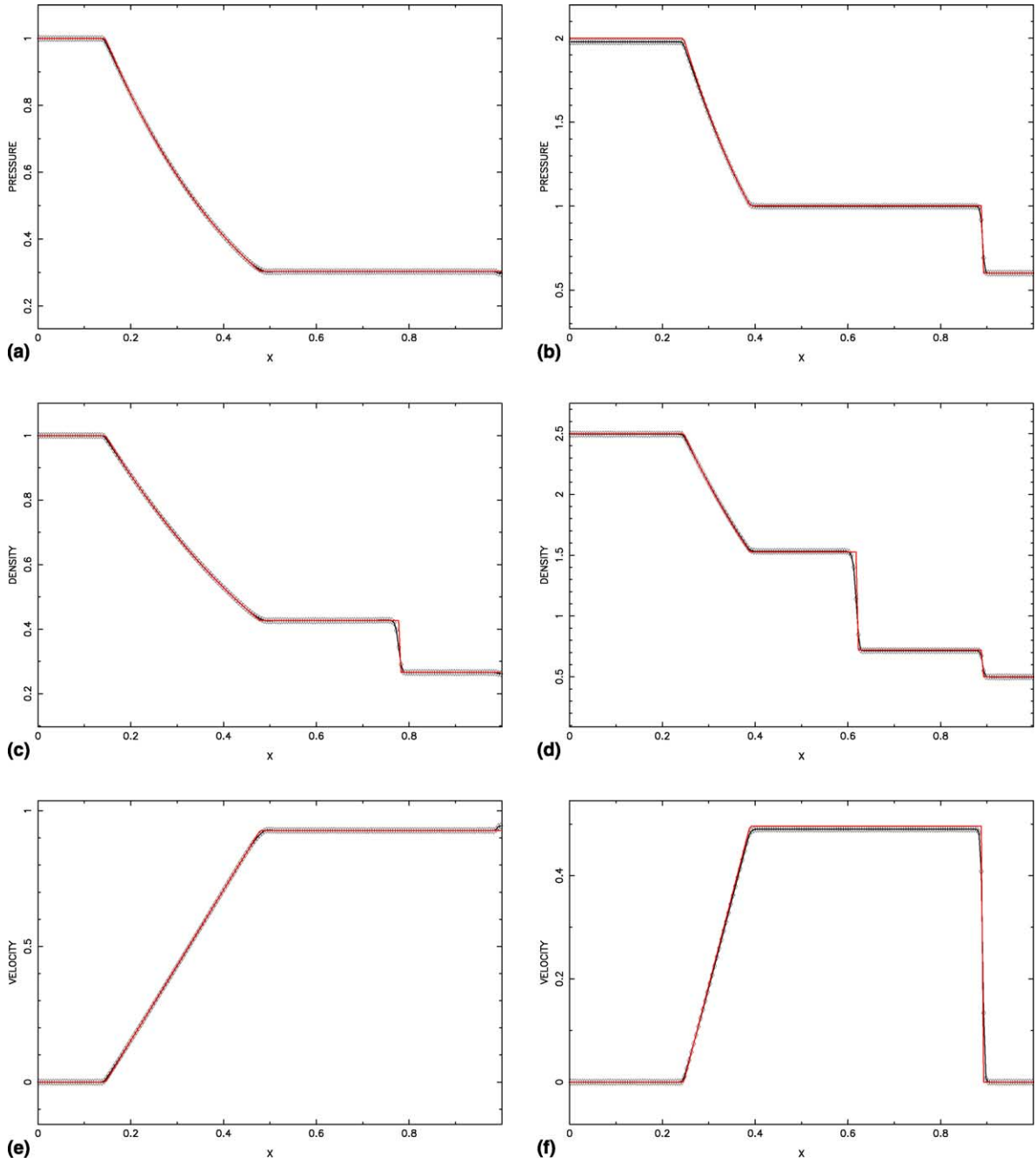


Fig. 4. Pressure, density and velocity: Numerical (\diamond) and analytical (thin line) solution of high-resolution model for the shock-tube problem at time = 0.30 (a), (c) and (e); observations (red line) and numerical solution of nonsmooth optimization (\diamond) for the high-resolution model at time = 0.24 for the second set of observations (b), (d) and (f).

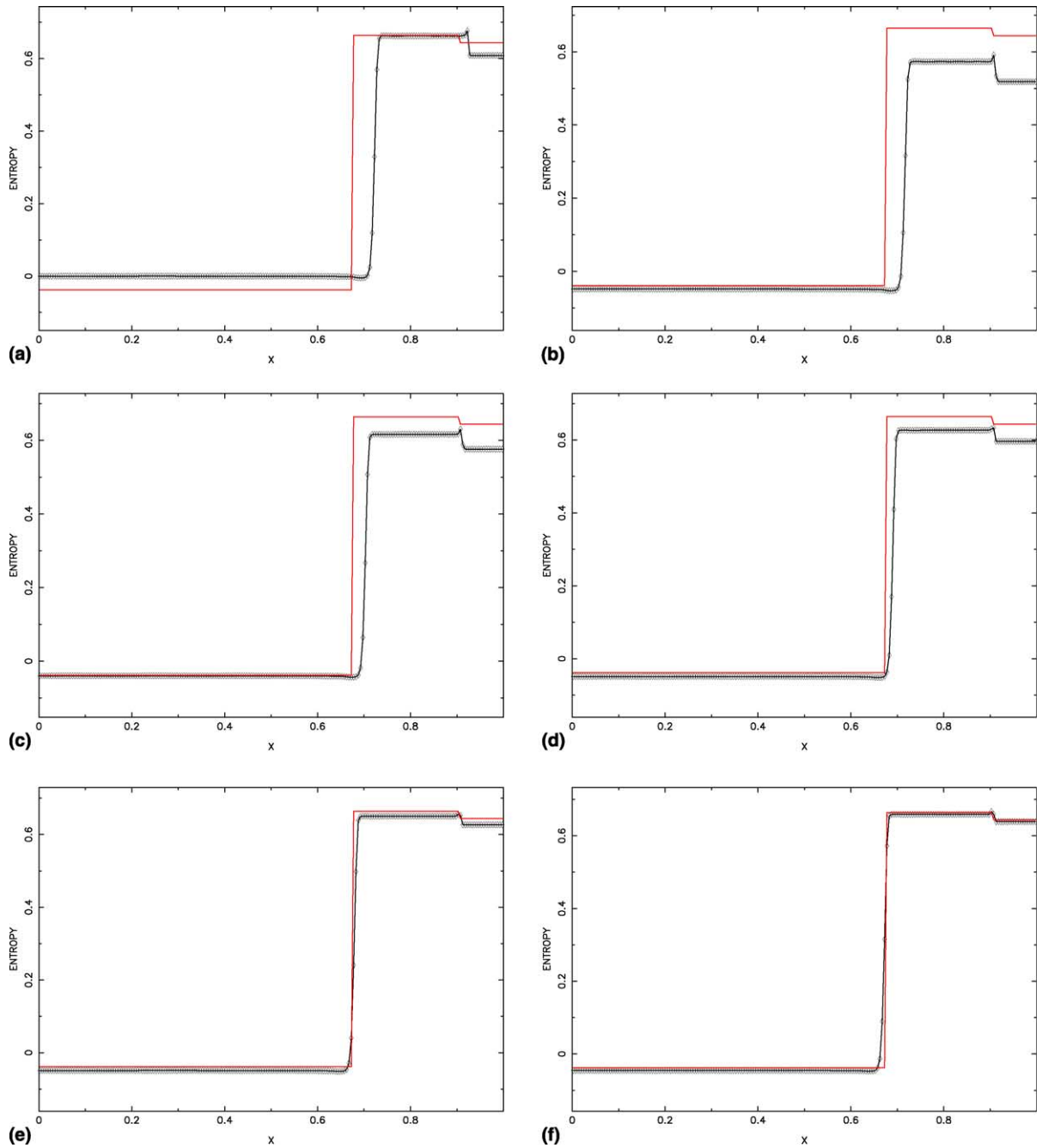


Fig. 5. Evolution of numerical (\diamond) and analytical (thin line) entropy (shown at final time $t = 0.24$ for the high-resolution model and for the first set of observations) during nonsmooth minimization: (a) iteration = 0, (b) iteration = 5, (c) iteration = 10, (d) iteration = 15, (e) iteration = 20 and (f) iteration = final iteration.

The L-BFGS minimization converged to the *desired* parameters only for the shorter time window ($T_W = 0.15$). For the larger time window ($T_W = 0.24$) the L-BFGS minimization failed. We explore in more detail this failure at the end of this section.

7.2. Numerical results for the artificial viscosity model AVM

We also applied successfully the nonsmooth minimization algorithm PVAR to the artificial viscosity model AVM which represents the class of models which *smooth* the discontinuities (see Table 4).

As seen in Table 4, L-BFGS converged only for the time window $T_W = 0.15$. For the larger time window $T_W = 0.24$ L-BFGS proved useful in a different setting. By using the L-BFGS output as an initial guess for the PVAR method we obtained convergence to the *desired* parameters in fewer minimization iterations. The values of the control parameters obtained using this approach are shown in the row PVAR [*input*] of Table 4.

To alleviate the impact of discontinuities we tested a method whereby we removed from the cost functional the terms computed at the discontinuities. The shock discontinuities were found using the discontinuity detection method presented in Section 6. Since the shock location changes in the forward model after each minimization iteration it was necessary to apply the method of discontinuity detection at each iteration.

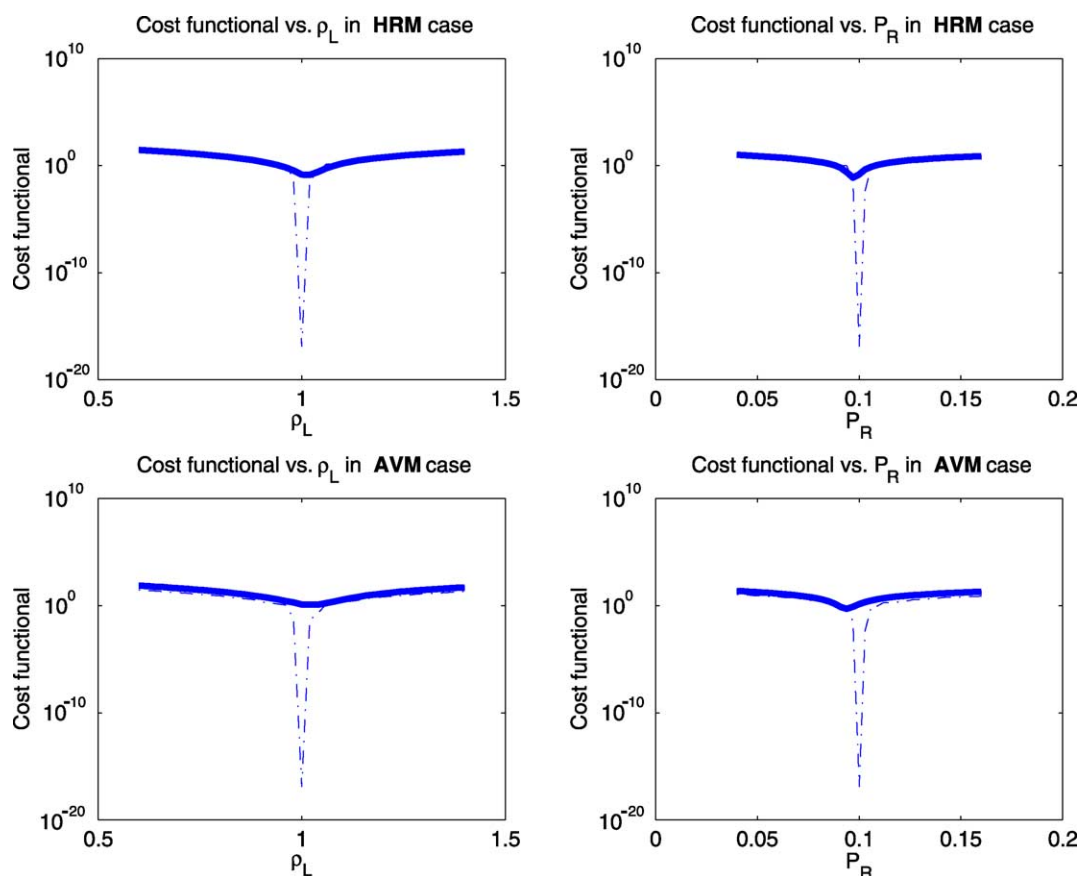


Fig. 6. The numerical (solid line) and analytical (dashed line) value of the cost functional $J(\rho_L, p_L, \rho_R, p_R)$ in a neighborhood of the initial guess for the control parameters $\text{INIT} = [\rho_L = 1.0, p_L = 1.0, \rho_R = 0.1, p_R = 0.1]$.

After removal of the aforementioned terms, the minimization was successful (see row L-BFGS [t.r] (term removal) of Table 4). One can notice that the solution obtained after minimization was more accurate compared to L-BFGS without term removal, especially for the larger time window. This may suggest that this approach should be employed for smooth minimization methods if the minimization gives a solution which is not “close enough” to the desired solution.

7.3. Additional numerical considerations

The control variables employed for this research were the initial values for only the pressure and density. Additional consideration would be required if we add the initial values for the velocity to the control variables. This is based on the fact that many decisions in the numerical model are based on the sign of the velocity. As a consequence, if one would choose the initial values of the velocity as part of the control variables one may expect that during the minimization their updates may have values which are not physical. One should also keep in mind that their corresponding adjoint variables may lead to solutions developing bifurcation points [15].

One may argue that the distance between the first or second set of parameters (ONE) and the initial guess (INIT) is rather small. But Fig. 1 shows large differences in the location of discontinuities and the

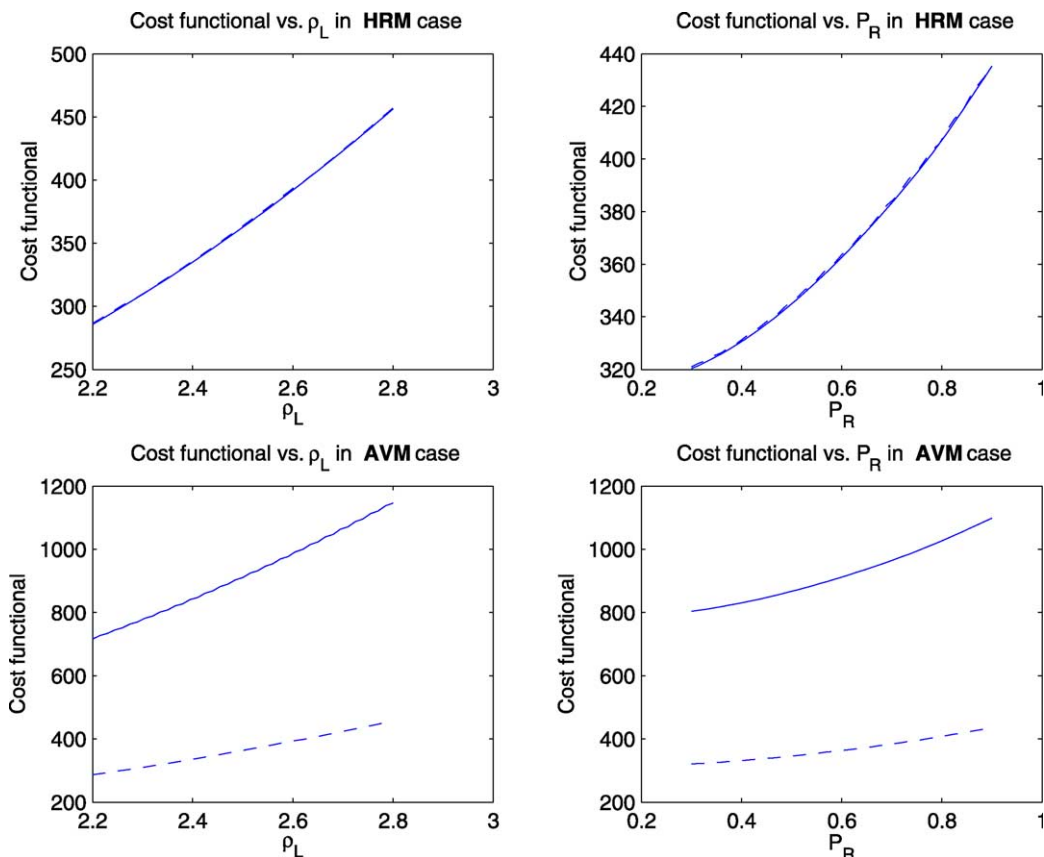


Fig. 7. The numerical (solid line) and analytical (dashed line) value of the cost functional $J(\rho_L, p_L, \rho_R, p_R)$ in a neighborhood of the second set of parameters TWO = $[\rho_L = 2.5, p_L = 2.0, \rho_R = 0.5, p_R = 0.6]$.

values for the flow variables for the corresponding flows, which provides a good argument for our choice. The second set of parameters (TWO) was chosen to be at a much larger distance to the initial guess (INIT) in order to test the robustness of our approach.

Figs. 6 and 7 show that the nonsmoothness of the cost functional appears only if the location of discontinuities of state and data coincide. But this does not translate into a successful run of the smooth optimization method L-BFGS.

Some of the reasons of failures of the L-BFGS method for our problem are discussed below.

For some cases (e.g., for HRM model using the first set of observations and time window $T_w = 0.24$) one can notice that the optimization criteria were satisfied (decrease of the cost functional), but the updated vector of control variables did not qualify as a solution from the physical point of view.

But we consider that the main reason behind this failure was given by the fact that the numerical values of the gradient of the cost functional did not converge to the analytical values as the number of grid points was increased for both models: HRM – Table 1 – and AVM – Table 2.

But although the convergence was not achieved, the fact that these values were in a “close enough” provided enough information for the nonsmooth optimization method PVAR to be successful even for the cases where L-BFGS did not work.

8. Summary and conclusions

We solved an optimal control problem for a flow which includes several types of discontinuities (namely we carried out a flow matching for a 1-D Riemann problem for Euler equations: shock-tube problem). The control variables considered were the initial conditions at the left and at the right of the membrane for pressure and density. Existence results were proved for the solution of the optimal control problem considered here. The cost functional was taken to be the (weighted) difference between the numerical and the *desired* solution of the model. The observations were taken either at the end of the time window or they were time distributed within the assimilation time horizon.

For the present problem flow matching was equivalent to relocation of discontinuities to a desired location. Since in all practical control applications discontinuities are captured using either high-resolution models or models which *smooth* the solution we employed here two numerical models representative of both approaches. For each forward code its corresponding discrete adjoint model was then employed for computing the gradient (or a subgradient) of the cost functional required for carrying out the minimization of the cost functional (using either nonsmooth or smooth algorithms for minimization). The two assimilation windows for minimization were chosen such that the flow with discontinuities retained all its characteristics at the end of each time window. If we were to use a slightly larger time window the model time evolution will change some of the characteristics of discontinuities.

The method of nonsmooth optimization (PVAR) employed for minimizing the cost functional was found to be very robust. For each of the different sets of observations employed we obtained optimized values of the control parameters in very good agreement with the *desired* results. The smooth minimization algorithm (L-BFGS) provided good results for the shorter time window and failed for the longer time window even after scaling the gradient of the cost functional. Better results for L-BFGS minimization were obtained when we removed from the cost functional the observations terms corresponding to the shock points, identified using a method of discontinuities detection.

The cost functional is nonsmooth only if the location of discontinuities and data coincide, which may suggest a good behavior of smooth optimization algorithms outside a close neighborhood of that location. But this behavior was not observed in our numerical simulation. We consider that the main reason behind the L-BFGS failure is the fact that the numerical values of the gradient, computed by the adjoint method, do not converge to the analytical values as the number of grid points is increased. But being “close enough” to

the analytical values provides sufficient information for the nonsmooth optimization method to be successful, since this method employs subgradients and not gradients of the cost functional.

The evolution of the entropy during various stages of the minimization process shows that the numerical solution of the optimal control problem we obtained is a physical solution since the correct weak solution of the shock tube problem must satisfy the entropy condition.

A very useful characteristic of the methodology for optimal control for discontinuous flow presented in this article is the ease with which it can be implemented in applications where the forward model is already discretized.

Extending this approach to optimal control problems with discontinuities in 2-D or 3-D renders the adjoint method even more appealing computationally, due to the larger number of control parameters involved.

An important topic to be addressed in future research is related to the issue of noisy observations. One may expect in this case that the cost functional should have new components which will account for the effect of the noise.

We consider our research to be only a small step towards the complete solution of optimal control of problems with discontinuities. Although published results are rather few, one may foresee a growing number of research efforts dedicated to the numerical and theoretical study of this class of important optimal control problems.

Acknowledgements

The authors acknowledge the support from the School of Computational Science and Information Technology, Florida State University. They thank L. Luksan, R. Leveque, T. Cowan, G. Wahba and P. Wesseling for sharing their expertise. The authors thank their reviewers for their insightful comments, which proved to be very useful for a better presentation of the results. The second author acknowledges the support from the NSF Grant No. ATM-9731472 managed by Dr. Linda Peng whom he would like to thank for her support.

References

- [1] G.A. Addington, J.M. Hyatt, Control-surface deflection effects on aerodynamic response nonlinearities, AIAA Paper 4107 (2000).
- [2] W.K. Anderson, A. Venkatakrishnan, Aerodynamic design optimization on unstructured grids with a continuous adjoint formulation, *Comput. Fluids* 28 (1999) 443.
- [3] J.D. Anderson, *Fundamentals of aerodynamics*, McGraw-Hill Series in Aeronautical and Aerospace Engineering, McGraw-Hill, 2001, 912 pp.
- [4] E. Arian, M.D. Salas, Admitting the inadmissible: adjoint formulation for incomplete cost functionals in aerodynamic optimization, ICASE Report, vols. 97–69, 1997.
- [5] C. Bardos, O. Pironneau, A formalism for the differentiation of conservation laws, *C. R. Acad. Sci. Paris* 335 (10) (2000) 839.
- [6] C. Bardos, O. Pironneau, Derivatives and control in the presence of shocks, *CFD J.* 12 (1) (2003).
- [7] P.I. Barton, J.R. Banga, S. Galan, Optimization of hybrid discrete continuous dynamic systems, *Comput. Chem. Engrg.* 24 (2000) 2171.
- [8] T. Bein, H. Hanselka, E. Breitbach, An adaptive spoiler to control the transonic shock, *Smart Mater. Struct.* 9 (2) (2000) 141.
- [9] J. Birkmeyer, H. Rosemann, E. Stanewsky, Shock control on a swept wing, *Aerosp. Sci. Technol.* 4 (3) (2000) 147.
- [10] L.G. Birta, T.I. Oren, A robust procedure for discontinuity handling in continuous system simulation, *T. Soc. Comput. Simul.* 2 (3) (1985) 189.
- [11] J.F. Bonnans, J. Gilbert, C. Lemarechal, C. Sagastizabal, *Optimisation Numerique: Aspects Theoriques et Pratiques*, Springer, Paris, 1997.
- [12] A. Bressan, Hyperbolic systems of conservation laws in one space dimension, in: *Proceedings International Congress of Mathematicians*, Beijing, 2002.
- [13] A. Bressan, *Hyperbolic Systems of Conservation Laws. The One Dimensional Cauchy Problem*, Oxford University Press, Oxford, 2000 (264 p.).

- [14] A. Bressan, G. Crasta, B. Piccoli, Well-posedness of the Cauchy problem for $n \times n$ systems of conservation laws, *Memoirs A.M.S.* 694 (2000).
- [15] D.G. Cacuci, Global optimization and sensitivity analysis, *Nucl. Sci. Engrg.* 104 (1990) 78.
- [16] E.M. Cliff, M. Heinkenschloss, A.R. Shenoy, Adjoint-based methods in aerodynamic design optimization, in: *Computational Methods for Optimal Design and Control*, Birkhauser, Basel, 1996, p. 91.
- [17] E.M. Cliff, M. Heinkenschloss, A.R. Shenoy, On the optimality system for a 1-D Euler flow problem, *AIAA Paper 96-3993* (1996).
- [18] E.M. Cliff, M. Heinkenschloss, A.R. Shenoy, An optimal control problem for flows with discontinuities, *J. Optim. Theory Appl.* 94 (2) (1997) 273.
- [19] T.J. Cowan, private communication, 2001.
- [20] A. Dadone, M. Valorani, B. Grossman, Optimization of 2D fluid design problems with nonsmooth or noisy objective function, in: *Computational Fluid Dynamics '96*, Wiley, New York, 1996, p. 425.
- [21] A. Dadone, B. Grossman, Progressive optimization of inverse fluid dynamic design problems, *Comput. Fluids* 29 (2000) 1.
- [22] A. Dadone, B. Grossman, Fast convergence of inviscid fluid dynamic design problems, in: *Proceedings of ECCOMAS 2000*, Barcelona, September 11–14, 2000, Available from www.imamod.ru/jour/conf/ECCOMAS2000/pdf/148.pdf.
- [23] R. Fletcher, *Practical Methods of Optimization*, Wiley, New York, 1987, 450 pp.
- [24] P.D. Frank, G.Y. Shubin, A comparison of optimization-based approaches for a model computational aerodynamics design problem, *J. Comput. Phys.* 98 (1992) 74.
- [25] M.B. Giles, N.A. Pierce, Adjoint equations in CFD: duality, boundary conditions and solution behaviour, *AIAA Paper 97-1850* (1997).
- [26] M.B. Giles, N.A. Pierce, On the properties of solutions of the adjoint Euler equations, in: *Numerical Methods for Fluid Dynamics VI*, ICFD, Oxford, 1998.
- [27] M.B. Giles, N.A. Pierce, Analytic adjoint solutions for the quasi-1D Euler equations, *J. Fluid Mech.* 426 (2001) 327.
- [28] M.B. Giles, N.A. Pierce, An introduction to the adjoint approach to design, *Flow Turbul. Combust.* 65 (3–4) (2000) 393.
- [29] M.B. Giles, Discrete adjoint approximations with shocks, in: *Proceedings of HYP2002 Conference*, Caltech, March 2002.
- [30] E. Godlewski, P.A. Raviart, *Numerical Approximation of Hyperbolic Systems of Conservation Laws*, Springer, New York, 1996, 508 pp.
- [31] M. Gunzburger, Sensitivities, adjoints and flow optimization, *Int. J. Numer. Methods Fluid* 31 (1999) 53.
- [32] M. Gunzburger, Sensitivities in computational methods for optimal flow control, in: *Computational Methods for Optimal Design and Control*, Birkhauser, Basel, 1996, p. 197.
- [33] A. Habbal, Direct approach to the minimization of the maximal stress over an arch structure, *J. Optim. Theory Appl.* 97 (3) (1998) 551.
- [34] A. Habbal, Nonsmooth shape optimization applied to linear acoustics, *SIAM J. Optim.* 8 (4) (1998) 989.
- [35] E. Hassold, Automatic differentiation applied to a nonsmooth optimization problem, in: *Numerical Methods in Engineering '96*, Wiley, New York, 1996, p. 835.
- [36] C. Homescu, I.M. Navon, Z. Li, Suppression of vortex shedding for flow around a circular cylinder using optimal control, *Int. J. Numer. Methods Fluids* 38 (2002) 43.
- [37] C. Homescu, I.M. Navon, Numerical and theoretical considerations for sensitivity calculation of discontinuous flow, *Syst. Control Lett.* 48 (2003) 253.
- [38] L. Huyse, M.R. Lewis, Aerodynamic shape optimization of two-dimensional airfoils under uncertain conditions, *ICASE Report*, vol. 2001-1, 2001.
- [39] A. Iollo, M.D. Salas, Optimum transonic airfoils based on Euler equations, *Comput. Fluids* 28 (1999) 653.
- [40] A. Iollo, M.D. Salas, S. Ta'asan, Shape optimization governed by the Euler equations using an adjoint method, *ICASE Report*, vols. 93–78, 1993.
- [41] A. Iollo, M.D. Salas, Contribution to the optimal shape design of two-dimensional internal flows with embedded shocks, *J. Comput. Phys.* 125 (1) (1996) 124.
- [42] F. James, M. Sepulveda, Convergence results for the flux identification in a scalar conservation law, *SIAM J. Control Optim.* 37 (3) (1999) 869.
- [43] A. Jameson, A perspective on computational algorithms for aerodynamic analysis and design, *Prog. Aerosp. Sci.* 37 (2001) 197.
- [44] D. Lee, T. Pavlidis, One-dimensional regularization with discontinuities, *IEEE Trans. Pattern Anal. Machine Intell.* 10 (6) (1988) 822.
- [45] C. Lemarechal, Nondifferentiable optimization, subgradient and ϵ subgradient methods, in: *Optimization and Operations Research, Lecture Notes in Economics and Mathematical Systems*, 117, Springer, Berlin, 1976, p. 191.
- [46] C. Lemarechal, Nondifferentiable optimization, in: *Handbooks in Operations Research and Management Science*, vol. 1. Optimization, North-Holland, Amsterdam, 1989.
- [47] D. Leonard, N.V. Long, *Optimal Control Theory and Static Optimization in Economics*, Cambridge University Press, Cambridge, 1992, 368 pp.

- [48] R. Leveque, *Numerical Methods for Conservation Laws*, Birkhauser, Basel, 1992.
- [49] CLAWPACK: A Software Package for Conservation Laws and Hyperbolic Systems, Available from <http://www.amath.washington.edu/~rjl/clawpack>.
- [50] H.W. Liepmann, A. Roshko, *Elements of Gas Dynamics*, Wiley, New York, 1957.
- [51] D. Liu, J. Nocedal, On the limited memory BFGS method for large scale optimization, *Math. Program. B* 45 (1989) 503.
- [52] R. Lohner, K. Morgan, J. Peraire, M. Vahdati, Finite element flux-corrected transport (FEM-FCT) for the Euler and Navier–Stokes equations, *Int. J. Numer. Methods Fluids* 7 (1987) 1093.
- [53] L. Luksan, J. Vlcek, NDA: algorithms for nondifferentiable optimization, ICS Report, vol. 797, Institute of Computer Science, Academy of Sciences of the Czech Republic, 2000.
- [54] L. Luksan, J. Vlcek, Algorithm 811: NDA: algorithms for nondifferentiable optimization, *ACM T. Math. Software* 27 (2) (2001) 193.
- [55] M.M. Makela, P. Neittaanmaki, *Nonsmooth Optimization*, World Scientific, Singapore, 1992.
- [56] G. Mao, L.R. Petzold, Efficient integration over discontinuities for differential-algebraic systems, *Comput. Math. Appl.* 43 (2002) 65.
- [57] T. Matsuzawa, M. Hafez, Optimum shape design using adjoint equations for compressible flows with shock waves, *Int. J. Comput. Fluid D* 7 (3) (1998) 343.
- [58] T. Matsuzawa, M. Hafez, Treatment of shock waves in design optimization via adjoint equation approach, *Int. J. Comput. Fluid D* 7 (4) (1998) 405.
- [59] B. Mohammadi, O. Pironneau, *Applied Shape Optimization for Fluids*, Oxford Science Publications, Oxford, 2001, 368 pp.
- [60] R.P. Narducci, B. Grossman, R.T. Haftka, Sensitivity algorithms for an inverse design problem involving a shock wave, *Inverse Probl. Engrg.* 2 (1995) 49.
- [61] I.M. Navon, X. Zou, J. Derber, J. Sela, Variational data assimilation with an adiabatic version of the NMC spectral model, *Mon. Weather Rev.* 120 (1992) 1433.
- [62] J. Nocedal, Updating quasi-Newton matrices with limited storage, *Math. Comput.* 151 (35) (1980) 773.
- [63] J. Nocedal, S.J. Wright, *Numerical Optimization*, Springer, Berlin, 1999, 600 pp.
- [64] A. Oyama, S. Obayashi, K. Nakahashi, Transonic wing optimization using genetic algorithm, *AIAA Paper* 97-1854 (1997).
- [65] T. Park, P.I. Barton, State event location in differential-algebraic models, *ACM Trans. Model. Comput. Simul.* 6 (2) (1996) 137.
- [66] H. Schramm, J. Zowe, A version of the bundle idea for minimizing a nonsmooth function: conceptual idea, convergence analysis, numerical results, *SIAM J. Optim.* 2 (1) (1992) 121.
- [67] F. Shakib, T.J.R. Hughes, Z. Johan, A new finite formulation for computational fluid dynamics: X. The compressible Euler and Navier–Stokes equation, *Comput. Methods Appl. Mech. Engrg.* 89 (1991) 141.
- [68] G.A. Sod, A survey of finite-difference methods for systems of nonlinear conservation laws, *J. Comput. Phys.* 27 (1) (1978) 1.
- [69] E. Stanewsky, Adaptive wing and flow control technology, *Prog. Aerosp. Sci.* 37 (2001) 583.
- [70] J.E. Tolsma, P.L. Barton, Hidden discontinuities and parametric sensitivity calculations, *SIAM J. Sci. Comput.* 23 (6) (2002) 1862.
- [71] M. Valorani, A. Dadone, Sensitivity derivatives for non-smooth or noisy objective functions in fluid design problems, in: *Numerical Methods for Fluid Dynamics*, vol. 5, Oxford Clarendon Press, 1995, p. 605.
- [72] S. Ulbrich, On the existence and approximation of solutions for the optimal control of nonlinear hyperbolic conservation laws, in: *Optimal Control of Partial Differential Equations (Chemnitz 1998)*, International Series of Numerical Mathematics, 133, Birkhauser, Basel, 1999, p. 287.
- [73] S. Ulbrich, A sensitivity and adjoint calculus for discontinuous solutions of hyperbolic conservation laws with source terms, *SIAM J. Control Optim.* 41 (3) (2002) 740.
- [74] S. Ulbrich, *Optimal control of nonlinear hyperbolic conservation laws with source terms*, Habilitation Thesis, Fakultät für Mathematik, Technische Universität München, January 2002.
- [75] S. Ulbrich, Adjoint-based derivative computations for the optimal control of discontinuous solutions of hyperbolic conservation laws, *Syst. Control Lett.* 48 (3–4) (2002) 309.
- [76] J. Vlcek, L. Luksan, Globally convergent variable metric method for nonconvex nondifferentiable unconstrained minimization, *J. Optim. Theory Appl.* 111 (2) (2001) 407.
- [77] Y.J. Wang, H. Matsuhisa, Y. Honda, Loads on lower limb joints and optimal action of muscles for shock reduction, *JSME Int. J. C-Mech. SY.* 42 (3) (1999) 574.
- [78] Q. Xu, Generalized adjoint for physical processes with parameterized discontinuities. Part I: Basic issues and heuristic examples Part II: Vector formulations and matching conditions, *J. Atmos. Sci.* 53 (8) (1996) 1123.
- [79] S. Zhang, X. Zou, J.E. Ahlquist, I.M. Navon, J. Sela, Use of differentiable and nondifferentiable optimization algorithms for variational data assimilation with discontinuous cost functions, *Mon. Weather Rev.* 128 (12) (2000) 4031.
- [80] S. Zhang, X. Zou, J.E. Ahlquist, Examination of numerical results from tangent linear and adjoint of discontinuous nonlinear models, *Mon. Weather Rev.* 129 (2001) 2791.
- [81] X. Zou, I.M. Navon, M. Berger, P.K. Phua, T. Schlick, F.X. LeDimet, Numerical experience with limited-memory quasi-Newton methods for large-scale unconstrained nonlinear minimization, *SIAM J. Optim.* 3 (3) (1993) 582.